AGU PUBLICATIONS

Geophysical Research Letters

RESEARCH LETTER
10.1002/2014GL059570

Key Points:
- GPS is used to determine changes in the storage of water and snow in California
- GPS is used to distinguish between hydrological models

Supporting Information:
- Readme
- Figure S1
- Figure S2
- Figure S3
- Figure S4
- Figure S5

Correspondence to:
D. F. Argus,
Donald.F.Argus@jpl.nasa.gov

Citation:
Argus, D. F., Y. Fu, and F. W. Landerer (2014), Seasonal variation in total water storage in California inferred from GPS observations of vertical land motion, *Geophys. Res. Lett.*, *41*, 1971–1980, doi:10.1002/2014GL059570.

Received 10 FEB 2014
Accepted 8 MAR 2014
Accepted article online 12 MAR 2014
Published online 31 MAR 2014
Corrected 22 APR 2014

This article was corrected on 22 APR 2014. See the end of the full text for details.

Seasonal variation in total water storage in California inferred from GPS observations of vertical land motion

Donald F. Argus[1], Yuning Fu[1], and Felix W. Landerer[1]

[1]Jet Propulsion Laboratory, California Institute of Technology, Pasadena, California, USA

Abstract GPS is accurately recording vertical motion of Earth's surface in elastic response to seasonal changes in surface water storage in California. California's mountains subside up to 12 mm in the fall and winter due to the load of snow and rain and then rise an identical amount in the spring and summer when the snow melts, the rain runs off, and soil moisture evaporates. We invert the GPS observations of seasonal vertical motions to infer changes in equivalent water thickness. GPS resolves the distribution of change in total water across California's physiographic provinces at a resolution of 50 km, compared to 200 km resolution from the Gravity Recovery and Climate Experiment. The seasonal surface water thickness change is 0.6 m in the Sierra Nevada, Klamath, and southern Cascade Mountains and decreases sharply to about 0.1 m east into the Great Basin and west toward the Pacific coast. GPS provides an independent inference of change in total surface water, indicating water storage to be on average 50% larger than in the NLDAS-Noah hydrology model, likely due to larger changes in snow and reservoir water than in the model.

1. Introduction

Water resources essential to California's urban and agricultural needs fall mostly as snow and rain in the mountains, far from the cities and farms. The precipitation occurs mostly in the winter, and water is stored for use as snowpack in the mountains, surface water in huge artificial reservoirs, and groundwater in aquifers. An extensive infrastructure of dams and aqueducts has been built to store water and transport it to the metropolitan areas [*Hanak et al.*, 2011, Figure 2.6]. Challenges and conflicts have arisen concerning the management of California's water resources as the demand grows and climate changes [*Hanak et al.*, 2011]. Elements of climate change such as drought threaten man's water supply (cf. California Climate Adoption Strategy 2009). Metropolitan Los Angeles is particularly dependent on distant water, as it imports two thirds of its water via aqueducts from the mountains.

Solid Earth deforms in elastic response to the load of water, snow, ice, and atmosphere. The elastic response to a surface load is specified by well-known Green's functions [*Farrell*, 1972] that are insensitive to the Earth structure assumed [*Wahr et al.*, 2013]. The elastic vertical motion of Earth's surface naturally resolves the distribution of mass at high spatial resolution. That is, elastic vertical motion decreases rapidly with distance from a load. For example, for a disk with a radius of 7 km, subsidence 20 km from the disk center is less than half that 10 km from the disk center (Figure 1). For a point load, $u = m \times a \times G(\Theta)$, where u is vertical displacement (in meters), m is the mass of the load (in kilograms), a is Earth's radius (in meters), and G is the Green's function of Θ, the angular distance between the point load and the location. We determined modified Green's function for a disk with a particular radius by numerically integrating evenly spaced point loads in the disk. We next determined vertical displacement at the location using the modified Green's function for a disk load.

In this study we use the dense network of GPS sites in California, together with solid Earth's known elastic response to a surface load, to infer the distribution of changes in total water storage. We focus on the seasonal water cycle. In California, snow and water at Earth's surface attain a maximum around 1 April (at the end of the winter) and a minimum around 1 October (at the end of the summer). From the GPS time series, we first determine the average seasonal vertical oscillation (the value of uplift in the spring and summer, or value of subsidence in the fall and winter) and then perform an inversion to infer the seasonal change in surface water thickness as a function of location.

We compare GPS observations of water storage to Gravity Recovery and Climate Experiment (GRACE) and hydrology models in two ways. First, we compare vertical motion of Earth's surface observed with GPS to that predicted by hydrology models. This method has the advantage that the comparison is at the native GPS

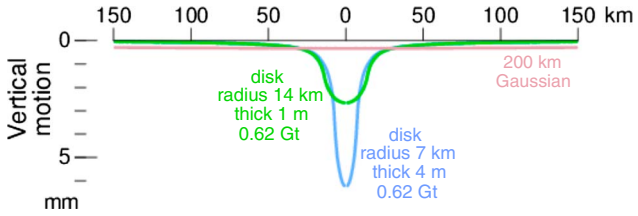

Figure 1. (Green curve) Vertical motion in elastic response to unloading of a disk with a radius of 14 km and a water thickness of 1 m. This disk has the same area as a pixel at 36°N that we estimate water thickness for (1/4° latitude by 1/4° longitude). (Blue curve) Vertical motion in elastic response to unloading of a disk with a radius of 7 km and a water thickness of 4 m. This disk has the same area as 1 NLDAS pixel at 36°N (1/8° latitude by 1/8° longitude). The Green's functions for PREM are used [*Wang et al*., 2012]. (Pink curve) Vertical motion that would be inferred by GRACE is approximated by a Gaussian distribution with a half width of 200 km. "Gt" is gigatons (10^{12} kg).

measurement. Second, we compare equivalent water thickness inferred from GPS to that inferred from GRACE and to that in hydrology models. Although there is uncertainty in the GPS inversion for surface water, we find the result to be robust because of the Green function property that the spatial distribution of surface mass is narrower than the spatial distribution of vertical motion. This method has the advantage that the comparison is at the level of interest to hydrologists.

We build on prior studies. Seasonal variation in snow in northeast Japan is known to produce uplift and subsidence at GPS sites [*Heki*, 2001]. GPS has accurately recorded changes in water and ice over areas just 10–20 km in diameter at Shasta Lake, California, and at Helheim and Midgaard Glaciers, Greenland [*Wahr et al*., 2013]. Snow thickness and soil moisture at GPS sites are being estimated from reflected signals (multipath) [*Larson et al*., 2008, 2009]. First steps toward evaluating surface water and groundwater in the western United States using GPS were taken by *Meertens et al*. [2012]. Seismicity and land uplift produced by groundwater loss in California's Central Valley is also being evaluated [*Amos et al*., 2014].

2. Methods

We analyze observations and models of vertical motion and total surface water storage change by performing seven steps:

1. We determine the seasonal vertical oscillation of all GPS sites in California and Nevada. A position, a velocity, and a sinusoid with a period of 1 year are fit to the GPS positions as a function of time. The mean vertical motion in the spring and the summer, from 1 April to 1 October, is the peak-to-peak amplitude of the sinusoid and taken to represent the mean seasonal vertical oscillation.
2. We identify and omit GPS sites on top of aquifers. These GPS sites record the porous response of solid Earth to groundwater filling and emptying the aquifers.
3. We fit a continuous, curved surface to the GPS observations of the seasonal vertical oscillations due to the loading of water and snow.
4. We invert the seasonal vertical oscillations observed with GPS to infer change in total surface water. The well-known Green's functions are used to relate vertical motion to mass change.
5. We compare the change in total surface water inferred from GPS to that observed with GRACE.
6. We compare the change in total surface water inferred from GPS to that in three hydrology models. The prediction of solid Earth's elastic response to loading in the hydrology models is also calculated and compared to the GPS observations of the seasonal vertical oscillation.
7. We evaluate the impact of seasonal oscillations in the weight of the atmosphere.

2.1. Determine the Seasonal Vertical Oscillation of GPS Sites

GPS time series of positions are from Jet Propulsion Laboratory's (JPL) reanalysis of all satellite orbits, clocks, and site positions from 1994 to 2013 [*Desai et al*., 2011]. JPL's GPS solution incorporates satellite phase center variations (igs08.atx) [*Schmid et al*., 2010] and improved solar radiation models [*Sibthorpe et al*., 2010]. This JPL solution is more accurate than prior solutions, as evident in a straighter series [*Argus*, 2012] for the scale transforming GPS positions into ITRF2008 [*Altamimi et al*., 2011]. That the series for scale is more nearly a straight line suggests that previous biases due to changing GPS satellite block types have disappeared. The improved accuracy allows solid Earth's elastic response to the loading of snow and water to be better determined. JPL's solution is available at ftp://sideshow.jpl.nasa.gov/pub in the directories JPL_GPS_Products and JPL_GPS_Timeseries/repro2011b.

We fit each GPS series with a position, a velocity, a sinusoid with a period of 1 year, and offsets when and where needed. The methods of *Argus et al.* [2010, Appendix B] are followed, except that the phase of the sinusoid of the east, north, and up components is allowed to differ. A total of 1069 GPS sites in California, Nevada, Oregon, and Washington are fit. Eighty percent of the GPS sites are from the Plate Boundary Observatory (PBO).

Most of the GPS sites have data starting between 2004 and 2008 continuing through to the present day. The median time period of observation is 7 years; 600 of the PBO sites have data from roughly 2007 to the present. Most of the 250 GPS sites in the Southern California Integrated GPS Network, which is now part of PBO, have data going back to 1999 or 2000.

2.2. Identify and Omit GPS Sites on Top of Aquifers

In most of California, vertical motion reflects solid Earth's elastic response to the loading of snow and water. Earth's surface subsides in the winter when loaded by snow and rain. The ground rises in the summer when the load dissipates.

Earth's surface at the top of an aquifer, however, responds differently. An aquifer expands as water fills the porous gravel, sand, and silt in the aquifer, causing Earth's surface to rise. Earth's surface rises in the winter when the aquifer is recharged with water and subsides in the summer when groundwater is withdrawn from the aquifer. Thus, Earth's porous response to groundwater is opposite to Earth's elastic response to the loading of snow and rain. Whereas the majority of GPS sites in California attain their maximum height at the end of the summer when the load of snow and rain has disappeared, the minority of GPS sites on top of aquifers attain their maximum height in the winter.

A total of 1069 GPS sites are analyzed. Primarily, 922 sites (86% of the total) record the loading of solid Earth by snow and surface water and are inverted for equivalent water thickness (Figure S1 in the supporting information, black vectors).

A total of 147 sites (14% of the total) are inferred to be significantly influenced by groundwater and omitted. Ninety two of these sites are omitted on the basis of the time of maximum height (the value of height calculated from the sinusoid fit to the vertical data is larger than 1 mm on 1 April) (Figure S1, red vectors). Forty-five sites are omitted on the basis of having a subsidence rate faster than -3 mm/yr (Figure S1, blue squares). Twenty-five omitted sites meet the criteria for both height time and subsidence rates. An additional 35 sites (3% of the total) are omitted on the basis of having a seasonal oscillation that is an outlier relative to nearby sites (Figure S1, violet vectors). Nearly all of the GPS sites in the aquifer category are within 5 km of a water well in the database of 20,000 wells that we obtained from the Department of Water and Power and the Metropolitan Water District of Los Angeles (Figure S1, tiny light blue dots).

The criteria that we apply result in a conservative assignment of sites to the loading category and a liberal assignment of sites to the aquifer category. While some sites recording primarily loading may be omitted, applying the criteria increases the accuracy of the inversion for water thickness.

2.3. Fit a Surface to the GPS Seasonal Vertical Oscillations

A continuous, curved surface is next fit to the GPS estimates of the mean seasonal vertical motion from 1 April to 1 October using the Generic Mapping Tool (GMT) program Surface [*Wessel and Smith*, 1998]. The Surface program implements a standard Laplacian technique for fitting a surface to data. The tension factor, T, specifying the curvature of the surface is assigned a standard value of 0.25. This results in a reasonable fit to the GPS vertical estimates without there being too much lateral variation in the surface.

2.4. Invert Vertical Motion for Equivalent Water Thickness

The GPS seasonal vertical oscillations are inverted for seasonal change in equivalent water thickness as a function of location by simultaneously minimizing the misfit of the model to the data and a Laplacian term limiting differences in water thickness between neighboring pixels. Values of equivalent water thickness are estimated at 1/4° intervals of latitude and longitude. Green's functions [*Wang et al.*, 2012] based on the preliminary reference Earth model (PREM) [*Dziewonski and Anderson*, 1981] are used to calculate solid Earth's

elastic response to a mass load. Each pixel is approximated using a circular disk of mass with a radius of about 14 km. We minimize the following:

$$(\mathbf{Ax}-\mathbf{b})/\boldsymbol{\sigma})^2 \quad + \quad \beta^2(L\,(\mathbf{x}))^2$$

where **b** is the vector of GPS observations of the seasonal vertical oscillation, **σ** is the vector of standard errors, **x** is the vector of surface water mass at each pixel, **A** is the design matrix consisting of the Green's functions relating the surface water mass at a pixel to the GPS vertical observation, *L* is the Laplacian operator, and β is a roughness factor specifying how much the value of neighboring pixels may differ. The bounded-value least squares algorithm of *Stark and Parker* [1995] is implemented. The *Stark and Parker* [1995] algorithm has also been used to estimate the distribution of slip along faults during great earthquakes [*Price and Burgmann*, 2002; *Elliot et al*., 2007; *Fu and Freymueller*, 2013].

A roughness factor, β, of 3 is found to result in a reasonable fit to the data. A smaller value of β would result in more variation in water thickness between neighboring pixels than warranted by the GPS data uncertainties. A larger value of β would result in insufficient lateral variation in water thickness to adequately fit the GPS data.

2.5. Compare Against GRACE Gravity

GRACE gravity estimates as a function of time are from the spherical harmonic coefficients in the Center for Space Research's Release-5, Level-2 solution (ftp://podaac.jpl.nasa.gov/allData/grace/L2/RL05). Standard practices are followed. The degree-1 coefficients estimated from the GRACE [*Swenson et al*., 2008] data and ocean models are added. The C20 coefficients estimated from SLR [*Cheng et al*., 2013] are substituted.

To be consistent with the GPS observations of surface loading, the Atmosphere and Ocean De-aliasing Level 1B model is added back to the GSM solution [*Fu et al*., 2012]. Gaussian smoothing using a half wavelength of 200 km is applied to reduce errors at high spherical harmonic degree [*Wahr et al*., 1998].

We fit a constant, a rate, and a sinusoid with a period of 1 year to series for each GRACE spherical harmonic coefficient. The estimated sinusoid parameters are expanded and used to infer seasonal change in water thickness. Solid Earth's elastic response to surface mass is estimated using *Kusche and Schrama* [2005, equation 6].

2.6. Compare Against the Seasonal Change in Total Water in Hydrology Models

The GPS inference of change in seasonal water thickness is compared against that in three hydrology models.

NLDAS-Noah is the North American Global Land Assimilation System [*Mitchell et al*., 2004]. The model includes values of terrestrial water storage, which is the sum of soil moisture and snow water equivalent, every month at 1/8° intervals of latitude and longitude.

GLDAS-Noah is the Global Land Data Assimilation System [*Rodell et al*., 2004]. The model specifies values of terrestrial water storage every month at 1° intervals of latitude and longitude. GLDAS is used to calculate GRACE gain factors to account for signal leakage [*Landerer and Swenson*, 2012]. The NLDAS and GLDAS models do not include either reservoir water or groundwater.

We construct a composite hydrology model consisting of soil moisture from NLDAS-Noah, snow water equivalent from Snow Data Assimilation System (SNODAS) [*National Operational Hydrologic Remote Sensing Center*, 2004], and surface water in 174 artificial reservoirs from *California Data Exchange Center* (*CDEC*) [2014]. This model follows that of *Famiglietti et al.* [2011] except that soil moisture is from NLDAS, not GLDAS. Snow Telemetry (SNOTEL) measurements indicate snow water equivalent in the Sierras to be 0.5–1.0 m thicker than in NLDAS-Noah [*Pan et al*., 2003, Figures 1 and 2]. Our composite model incorporates the SNODAS model that is fit to the SNOTEL measurements. In the composite model, the CDEC value of reservoir water volume was added to the 1/8°-square NLDAS pixel that the reservoir is in. The seasonal oscillation in reservoir water in the pixel at Shasta Lake (12 m) is 30 times greater than the maximum seasonal water oscillation in NLDAS.

A constant, a change rate, and a sinusoid are fit to the monthly values of total surface water in each of the three hydrology models. Values of water thickness in the hydrology models from 2007 through 2012 are fit, the time period that most closely matches that of the GPS observations. Solid Earth's elastic response to water change in the model was calculated from the Green's functions assuming PREM [*Wang et al*., 2012]. A disk

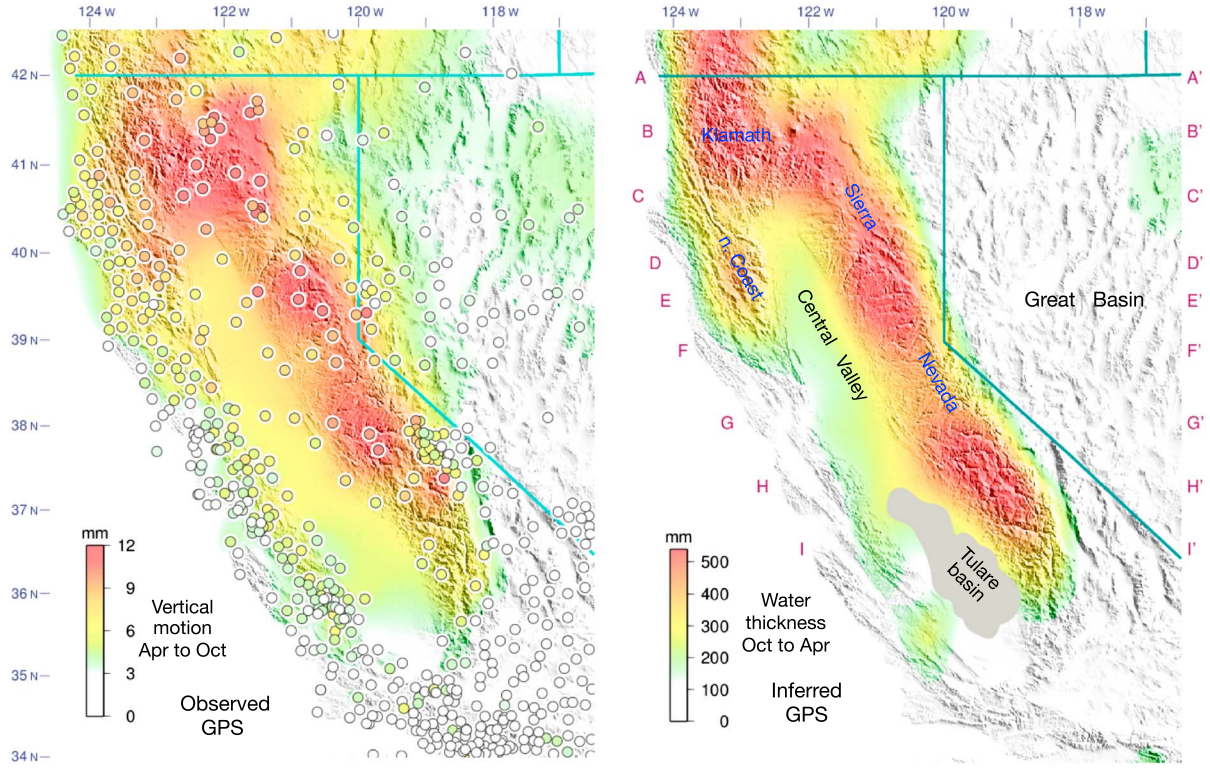

Figure 2. (left) Average uplift in the spring and summer observed with GPS is compared with (right) the inferred average increase in equivalent water thickness in the fall and winter. (Figure 2, left) Average uplift at GPS sites (circles) from 1 April to 1 October. The colors of the circles indicate the value of uplift. Seasonal uplift throughout California and Nevada (color gradations) is inferred by fitting a continuous, curved surface to the GPS estimates using GMT program Surface. (Figure 2, right) Average increase in equivalent water thickness (color gradations) from 1 October to 1 April is inferred by inverting the GPS vertical estimates as described in the main text. Seasonal water change in the Tulare basin (shaded gray) is poorly constrained by GPS. The letters (A through I) are at the endpoints of the cross sections along lines of constant latitude in Figure 4 and S4.

with the area of each pixel and the water thickness change from the hydrology model is used. At 36°N, the disk radii are 7.05 km.

2.7. Evaluate the Impact of the Atmosphere

Estimates of atmospheric pressure are from the ERA-Interim reanalysis of the (ECMWF) European Centre for Medium-Range Weather Forecast model [*Dee et al.*, 2011]. ECMWF has atmospheric pressure estimates at 3/4° intervals of latitude and longitude. Surface mass is calculated by multiplying atmospheric pressure by 9.81 m/s^2. Seasonal oscillations in equivalent water thickness due to atmospheric moisture are calculated by fitting monthly values in a fashion identical to that for the hydrology models.

3. Results

The seasonal vertical motion observed by GPS and the seasonal change in water thickness inferred from GPS are next compared to that predicted by the hydrology models.

3.1. GPS

GPS well resolves seasonal water storage across California (Figures 2, 4, and S4). Water storage is largest in California's mountains, which in the spring and summer are observed to rise 8–12 mm, in elastic response to snow melt, water runoff, and evaporation of 0.5–0.6 m of equivalent water thickness. Seasonal uplift and subsidence decreases sharply to less than 3 mm in the Great Basin and toward the Pacific coast.

GPS well resolves the distribution of seasonal water storage between California's physiographic provinces. Seasonal vertical oscillations and water thickness change are next described along nine lines of constant

latitude (Figures 4 and S4). The seasonal water change in the Klamath and southern Cascade Mountains (profiles B-B′ and C-C′) is inferred to be about 0.5 m on the basis of seasonal vertical oscillations of about 10 mm. The seasonal water change throughout the Sierra Nevada Mountains (profiles D-D′ through H-H′) is also inferred to be 0.5 m on the basis of seasonal vertical oscillations of 10 mm. A local maximum in water storage in the northern Coast Ranges north of San Francisco (profiles D-D′ and E-E′) is inferred from GPS to be 0.4 m and is separated from the Sierras water maximum by a local water storage minimum in the northern Central Valley (profiles D-D′ and E-E′).

Water storage decreases sharply from the Sierra Nevada Mountains east into the desert of the Great Basin. The seasonal vertical oscillation decreases from 10 mm in the Sierras to less than 2 mm in the Great Basin over a distance of less than 50 km. Seasonal water storage in most of the Great Basin is inferred with GPS to be about 0.1 m. The decline in the vertical seasonal oscillation is similarly sudden going west from the central and northern Coast Ranges toward the Pacific coast.

GPS poorly constrains seasonal water storage in the southern Central Valley because sites there are on top of the aquifer. The Tulare river basin is observed with GPS to subside at a long-term rate of at least 5 mm/yr (shaded gray in Figure 2 (right)), with subsidence in places of up to 0.15 m/yr due to groundwater depletion (Figure S1).

Vertical oscillations at several GPS sites in the northern Central Valley are observed to be 5–8 mm with maximum height around 1 October, suggesting seasonal water storage there to be about 0.3–0.4 m. Seasonal oscillations in groundwater averaged over the entire Central Valley in a typical year are estimated from water well data and aquifer models to be about 0.15 m [*Faunt*, 2009, Figure B5] (8 km^3/58,000 km^2 = 0.14 m).

3.2. Comparison to GRACE

GRACE, with satellites at an altitude of 400 km, does not resolve the spatial distribution of water storage across California very well. (Figure S3 (top right), 4, and S4). GRACE estimates of seasonal water thickness change decrease gradually from California's mountains east to the Great Basin. In the Sierras, the seasonal water storage is estimated by GRACE to be just 0.2 m, smaller than the true water storage because the signal leaks east into the Great Basin and west into the Pacific Ocean. In the western Great Basin, water storage estimated by GRACE is 0.15 m, larger than truth. In practice, GRACE estimates of total water change in the Sacramento-San Joaquin River basin is adjusted by a scaling factor of 2 or 3 based on the GLDAS hydrology model to account for leakage [*Famiglietti et al*., 2011; *Landerer and Swenson*, 2012].

3.3. Comparison to Hydrology Models

Seasonal water storage in California's mountains inferred from GPS is on average about 50% greater than in hydrology model NLDAS-Noah (Figures 3, 4, and S4). In the Klamath Mountains, seasonal water change inferred from GPS is up to 0.6 m, twice as big as in NLDAS. In the northern and southern Sierras, seasonal water storage inferred from GPS is 0.6 m, also larger than in NLDAS. In the western Great Basin, seasonal water change from GPS is about 0.1 m, roughly equal to that in NLDAS.

In GLDAS-Noah, water thickness is specified at just 1° intervals of latitude and longitude, giving a more coarse description of total surface water than NLDAS (second page of Figure S3 and Figures 4 and S4). In the Klamath Mountains and southern Cascade Ranges, seasonal water change in GLDAS is 0.4 m, closer to the GPS-inferred value of 0.6 m than NLDAS. In the Sierra Nevada Mountains, seasonal water change in GLDAS-Noah is 0.3 m and, like NLDAS, is smaller than inferred from GPS.

The composite model, consisting of NLDAS soil moisture, SNODAS snow, and CDEC reservoir water, has overall total water storage about equal to that inferred from GPS (Figures 3, 4, and S4). In the Sierra Nevada Mountains, total water storage is comparable between the composite model and that inferred from GPS, although the distribution of water thickness inferred from GPS is broader than that in the composite model (in profiles F-F′ through I-I′). In the Klamath Mountains, however, seasonal water change inferred from GPS of 0.6 m is twice as big as in the composite model.

3.4. Evaluation of Atmospheric Loading

Whereas GPS and GRACE record the total surface load (oceans, continental water, and atmosphere), the hydrology models have only continental water. Earth's surface moves several millimeters in response to

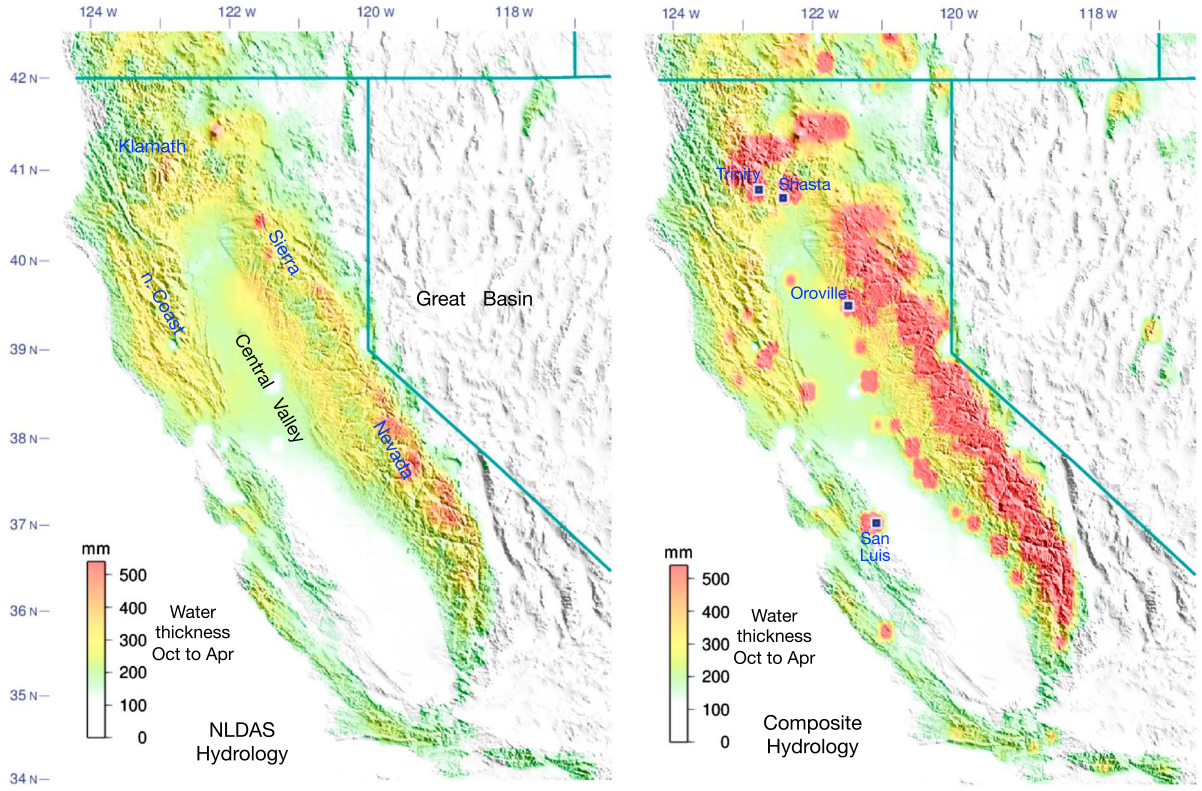

Figure 3. Average increase in equivalent water thickness (color gradations) in the fall and winter in the (left) NLDAS-Noah and (right) composite hydrology models. The average increase in water thickness from 1 October to 1 April is calculated from the sinusoid fit to data in the hydrology models from 2007 through 2012. The composite model consists of soil moisture in NLDAS, snow water equivalent in SNODAS, and reservoir water in CDEC. The four artificial reservoirs with the largest seasonal oscillations are plotted (blue squares) at Figure 3 (right).

high- and low-pressure weather systems, but the range in height in California averaged over 1 month is typically no more than 3 mm. Moreover, atmospheric height changes are not sustained over the seasons. In ECMWF's ERA-Interim reanalysis [*Dee et al.*, 2011], the seasonal atmospheric vertical oscillation from 1 April to 1 October ranges from 0.0 mm along the California coast to −1.2 mm in the central Great Basin (Figures 4, S4, and S5). If we were to adjust for atmospheric loading in ECMWF, the seasonal oscillation in water thickness inferred by GPS would increase by 0.05 m in the Great Basin. Seasonal vertical oscillations are also calculated to be small in the atmosphere model from the (NCEP) National Center for Environmental Prediction [*van Dam and Wahr*, 1987; geophy.uni.lu/ncep-loading.html].

4. Discussion

GRACE gravity observations have been used to infer that California's Central Valley lost 20 km^3 of groundwater from 2003 to 2010, for a loss rate of 3 km^3/yr [*Famiglietti et al.*, 2011]. We anticipate that GPS and GRACE will next be used together to more accurately estimate groundwater change. GRACE has the strength that it strongly constrains total water storage. GPS has the strength that it resolves solid Earth's elastic response to surface loading at high lateral resolution, thus constraining the distribution of snow and water. GPS will be used to determine total surface water change in the Sierra Nevada Mountains (soil moisture plus snow plus reservoir water), thus distinguishing between and further constraining the hydrology models. GRACE will then be used to more accurately determine groundwater change in the Central Valley using the hydrology model fit to the GPS data.

We expect horizontal motions of GPS sites to be capable of further constraining seasonal change in total water thickness [*Wahr et al.*, 2013; *Fu et al.*, 2013].

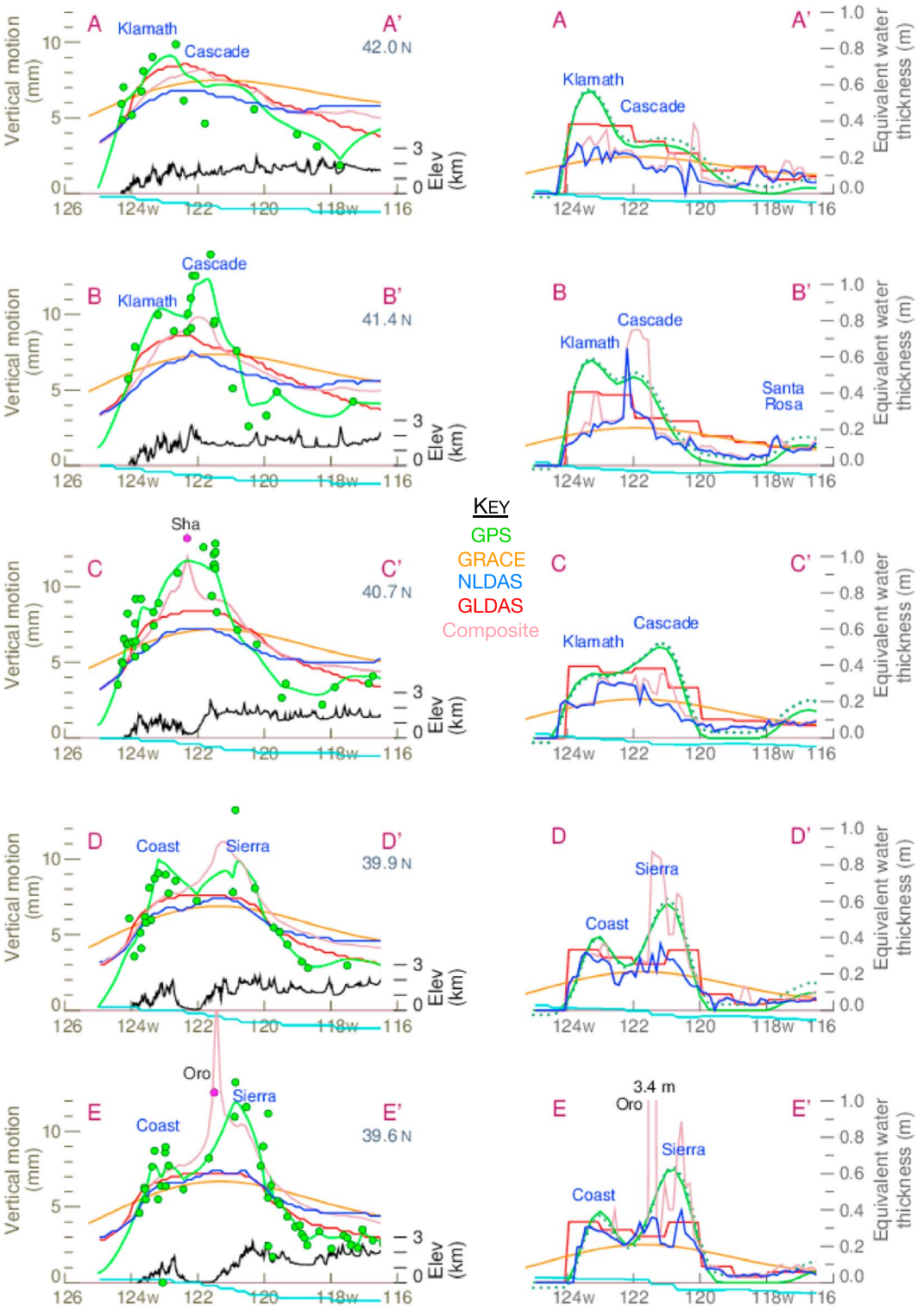

Figure 4. Profiles along lines of constant latitude (see Figure 2) of (left) average uplift in the spring and summer observed with GPS and (right) average increase in equivalent water thickness during the fall and winter. The curves are the following: (green) GPS, (orange) GRACE, (dark blue) NLDAS hydrology, (red) GLDAS hydrology, (pink) composite hydrology, (light blue) ERA-Interim ECMWF atmosphere model, and (dotted green) GPS corrected for ERA-Interim ECMWF. Average uplift at GPS sites (green circles) is from 1 April to 1 October. Observed average uplift at GPS sites at Shasta Lake ("Sha") and Lake Oroville ("Oro") is plotted as magenta circles. Elevation is plotted as the rugged black curve. The locations of the mountain ranges are printed in blue.

5. Conclusions

GPS has been used for 25 years to evaluate continental deformation and interseismic strain accumulation in California [e.g., *Argus and Gordon*, 2001; *Argus et al*., 2005; *d'Alessio et al*., 2005]. Seasonal vertical oscillations of aquifers in porous response to the recharge and withdrawal of groundwater have also been analyzed [e.g., *Bawden et al*., 2001; *Argus et al*., 2005]. In this study we demonstrate that vertical motion in most places in California records primarily solid Earth's elastic response to the loading of snow and surface water. Thus, UNAVCO Plate Boundary Observatory (PBO) of 900 GPS sites is of great use for evaluating water resources.

GPS observations of vertical displacement allow change in total water storage to be inferred. GPS resolves seasonal water storage across California's physiographic provinces at a spatial resolution of 50 km, compared to 200 km from GRACE. Seasonal water storage in the Klamath and in the Sierra Nevada Mountains is up to 0.6 m in equivalent water thickness and decreases sharply to about 0.1 m east into the Great Basin and west toward the Pacific coast. GPS distinguishes between hydrology models, requiring seasonal water storage to be larger than in NLDAS-Noah, but comparable in size to a composite model of soil moisture, snow, and reservoir water.

Acknowledgments

We appreciate the contribution of Michael Heflin, Angelyn Moore, Shailen Desai, and members of JPL's GPS data analysis team. We are grateful for the reviews of three anonymous scientists and for the suggestions of Roland Burgmann, Josh Fisher, Duane Waliser, and Editor Eric Calais. UNAVCO's Plate Boundary Observatory (PBO) and the International GNSS Service (IGS) provided the GPS observations. The GPS positions were determined as part of NASA's MEaSUREs project. This research was performed under contract by NASA at the Jet Propulsion Laboratory, California Institute of Technology. The GPS data used in this study are available at ftp://sideshow.jpl.nasa.gov/pub in the directories JPL_GPS_Products and JPL_GPS_Timeseries/repro2011b.

The Editor thanks three anonymous reviewers for their assistance in evaluating this paper.

References

Altamimi, Z., X. Collilieux, and L. Metivier (2011), ITRF2008: An improved solution of the international terrestrial reference frame, *J. Geod.*, *85*, 457–473, doi:10.1007/s011190-011-0444-4.

Amos, C. B., P. Audet, W. C. Hammond, R. Bürgmann, I. A. Johanson, and G. Blewitt (2014), Uplift and seismicity driven by groundwater depletion in central California, Nature, doi:10.1038/nature13275, in press.

Argus, D. F. (2012), Uncertainty in the velocity between the mass center and surface of Earth, *J. Geophys. Res.*, *117*, B10405, doi:10.1029/2012JB009196.

Argus, D. F., and R. G. Gordon (2001), Present tectonic motion across the Coast Ranges and San Andreas fault system in central California, *Geol. Soc. Am. Bull.*, *113*, 1580–1492.

Argus, D. F., M. B. Heflin, G. Peltzer, F. H. Webb, and F. Crampe (2005), Interseismic strain accumulation and anthropogenic motion in metropolitan Los Angeles, *J. Geophys. Res.*, *101*, B04401, doi:10.1029/2003JB002934.

Argus, D. F., R. G. Gordon, M. B. Heflin, C. Ma, R. J. Eanes, P. Willis, W. R. Peltier, and S. E. Owen (2010), The angular velocities of the plates and the velocity of Earth's center from space geodesy, *Geophys. J. Int.*, *180*, 913–960, doi:10.1111/j.1365-246X.2009.04463.x.

Bawden, G. W., W. Thatcher, R. S. Stein, K. W. Hudnut, and G. Peltzer (2001), Tectonic contraction across Los Angeles after removal of groundwater pumping effects, *Nature*, *412*, 812–815.

California Data Exchange Center (CDEC) (2014), California Data Exchange Center. [Available at http://cdec.water.ca.gov.]

Cheng, M. K., B. D. Tapley, and J. C. Ries (2013), Deceleration in Earth's oblateness, *J. Geophys. Res. Solid Earth*, *118*, 740–747, doi:10.1002/jgrb.50058.

d'Alessio, M. A., I. A. Johanson, R. Burgmann, D. Schmidt, and M. H. Murray (2005), Slicing up the San Francisco Bay Area: Block kinematics and fault slip rates from GPS-derived surface velocities, *J. Geophys. Res.*, *110*, B06403, doi:10.1029/2004JB003496.

Dee, D. P., et al. (2011), The ERA-Interim reanalysis: Configuration and performance of the data assimilation system, *Q. J. R. Meteorol. Soc.*, *137*, 553–597.

Desai, S. D., W. Bertiger, B. Haines, N. Harvey, D. Kuang, C. Lane, A. Sibthorpe, F. Webb, and J. Weiss (2011), Results from the reanalysis of the global GPS network, Fall 2009 AGU abstract G11B–0630.

Dziewonski, A., and D. L. Anderson (1981), Preliminary reference Earth model, *Phys. Earth Planet. Inter.*, *25*, 297–356.

Elliott, J. L., J. T. Freymueller, and B. Rabus (2007), Coseismic deformation of the 2002 Denali fault earthquake: Contributions from synthetic aperture radar range offsets, *J. Geophys. Res.*, *112*, B06421, doi:10.1029/2006JB004428.

Famiglietti, J. S., M. Lo, S. L. Ho, J. Bethune, K. J. Anderson, T. H. Syed, S. C. Swenson, C. R. de Linage, and M. Rodell (2011), Satellites measure recent rates of groundwater depletion in California's Central Valley, *Geophys. Res. Lett.*, *38*, L03403, doi:10.1029/2010GL046442.

Faunt, C. C. (Ed.) (2009), Groundwater availability of the Central Valley Aquifer, California *U.S. Geol. Surv. Prof. Pap.*, *1766*, Sacramento, Calif.

Farrell, W. E. (1972), Deformation of the Earth by surface loads, *Rev. Geophys.*, *10*, 761–797, doi:10.1029/RG010i003p00761.

Fu, Y., D. F. Argus, J. T. Freymueller, and M. B. Heflin (2013), Horizontal motion in elastic response to seasonal loading of rain water in the Amazon Basin and monsoon water in Southeast Asia observed by GPS and inferred from GRACE, *Geophys. Res. Lett.*, *40*, 6048–6053, doi:10.1002/2013GL058093.

Fu, Y., and J. T. Freymueller (2013), Repeated large slow slip events at the southcentral Alaska subduction zone, *Earth Planet. Sci. Lett.*, *375*, 303–311, doi:10.1016/j.epsl.2013.05.049.

Fu, Y., J. T. Freymueller, and T. Jensen (2012), Seasonal hydrological loading in southern Alaska observed by GPS and GRACE, *Geophys. Res. Lett.*, *39*, L15310, doi:10.1029/2012GL052453.

Hanak, E., J. Lund, A. Dinar, B. Gray, R. Howitt, J. Mount, P. Moyle, and B. Thompson (2011), *Managing California's Water, From Conflict to Reconcilliation*, Public Policy Institute of California, San Francisco, Calif.

Heki, K. (2001), Seasonal modulation of interseismic strain buildup in northeastern Japan driven by snow loads, *Science*, *293*, 89–92.

Kusche, J., and E. J. O. Schrama (2005), Surface mass redistribution inversion from global GPS deformation and Gravity Recovery and Climate Experiment (GRACE) gravity data, *J. Geophys. Res.*, *110*, B09409, doi:10.1029/2004JB003556.

Landerer, F. W., and S. C. Swenson (2012), Accuracy of scaled GRACE terrestrial water storage estimates, *Water Resour. Res.*, *48*, W04531, doi:10.1029/2011WR011453.

Larson, K. M., E. E. Small, E. D. Gutmann, A. L. Bilich, J. J. Braun, and V. U. Zavrotny (2008), Use of GPS receivers as a soil moisture network for water cycle studies, *Geophys. Res. Lett.*, *35*, L24405, doi:10.1029/2008GL036013.

Larson, K. M., E. D. Gutmann, V. U. Zavorotny, J. J. Braun, M. W. Williams, and F. G. Nievinski (2009), Can we measure snow depth with GPS receivers?, *Geophys. Res. Lett.*, *36*, L17502, doi:10.1029/2009GL039430.
Meertens, C., F. Blume, H. Burgland, C. Puskas, J. Wahr, T. van Dam, and T. Herring (2012), *Investigation of Non-Tectonic Signals at GPS Stations*, International GNSS Service workshop, Olsztyn, Poland.
Mitchell, K. E., et al. (2004), The multi-institution North American Land Data Assimilation System (NLDAS): Utilizing multiple GCIP products and partners in a continental distributed hydrological modeling system, *J. Geophys. Res.*, *109*, D07S90, doi:10.1029/2003JD003823.
National Operational Hydrologic Remote Sensing Center (2004), *Snow Data Assimilation System (SNODAS) Data Products at NSIDC*, Natl. Snow and Ice Data Cent., Boulder, Colo., U.S.A., doi:10.7265/N5TB14TC.
Pan, M., et al. (2003), Snow process modeling in the North American Land Data Assimilation System (NLDAS): 2. Evaluation of model simulated snow water equivalent, *J. Geophys. Res.*, *108*(D22), 8850, doi:10.1029/2003JD003994.
Price, E. J., and R. Bürgmann (2002), Interactions between the Landers and Hector Mine, California, earthquakes from space geodesy, boundary element modeling and time-dependent friction, *Bull. Seismol. Soc. Am.*, *92*(4), 1450–1469.
Rodell, M., et al. (2004), The global land data assimilation system, *Bull. Am. Meteorol. Soc.*, *85*, 381–394.
Schmid, R., X. Collilieux, F. Dilssner, R. Dach, and M. Schmitz (2010), *Updated Phase Center Corrections for Satellite and Receiver Antennas*, June 2010 IGS workshop presentation, Newcastle, England.
Sibthorpe, A., J. P. Weiss, N. Harvey, D. Kuang, and Y. Bar-Sever (2010), Empirical modeling of solar radiation pressure forces affecting GPS satellites, Abstract G54A-04 presented at 2010 Fall Meeting, AGU, San Francisco, Calif., 13–17 Dec.
Stark, P. B., and R. L. Parker (1995), Bounded-variable least-squares: An algorithm and application, *Comput. Stat.*, *10*(2), 129–141.
Swenson, S., D. Chambers, and J. Wahr (2008), Estimating geocenter variations from a combination of GRACE and ocean model output, *J. Geophys. Res.*, *113*, B08410, doi:10.1029/2007JB005338.
van Dam, T. M., and J. M. Wahr (1987), Displacements of the Earth's surface due to atmospheric loading: Effects on gravity and baseline measurements, *J. Geophys. Res.*, *92*, 1281–1286, doi:10.1029/JB092iB02p01281.
Wahr, J., M. Molenaar, and F. Bryan (1998), Time variability of the Earth's gravity field: Hydrological and oceanic effects and their possible detection using GRACE, *J. Geophys. Res.*, *103*(B12), 30,205–30,229, doi:10.1029/98JB02844.
Wahr, J., S. A. Khan, T. van Dam, L. Liu, J. H. van Angelen, M. R. van den Broeke, and C. M. Meertens (2013), The use of GPS horizontals for loading studies, with applications to northern California and southeast Greenland, *J. Geophys. Res. Solid Earth*, *118*, 1795–1806, doi:10.1002/jgrb.50104.
Wang, H., L. Xiang, L. Jia, L. Jiang, Z. Wang, B. Hu, and P. Gao (2012), Load Love numbers and Green's functions for elastic Earth models PREM, iasp91, ak135, and modified models with refined crustal structure from Crust 2.0, *Comp. Geosci.*, *49*, 190–199.
Wessel, P., and W. H. F. Smith (1998), New, improved version of generic mapping tools released, *Eos Trans. AGU*, *79*(47), 579, doi:10.1029/98EO00426.

Erratum

In the originally published version of this article, the sentence citing *Amos et al.* [2014] was incorrectly placed at the end of the abstract. In this corrected version, this sentence appears at the end of the Introduction.